Chi *et al. J. Mater. Inf.* **2025**, *5*, 11
DOI: 10.20517/jmi.2024.49

Journal of Materials Informatics

Research Article

Open Access

Check for updates

Design of Fe_2Mo@γ-GDY triatomic catalyst for electrocatalytic urea synthesis of N_2 and CO: a theoretical study

Linyuan Chi, Tonghui Wang*, Qing Jiang*

Key Laboratory of Automobile Materials (Jilin University), Ministry of Education, and School of Materials Science and Engineering, Jilin University, Changchun 130022, Jilin, China.

***Correspondence to:** Prof. Tonghui Wang, Prof. Qing Jiang, Key Laboratory of Automobile Materials (Jilin University), Ministry of Education, and School of Materials Science and Engineering, Jilin University, 5988 Renmin Street, Changchun 130022, Jilin, China. E-mail: twang@jlu.edu.cn; jiangq@jlu.edu.cn

How to cite this article: Chi, L.; Wang, T.; Jiang, Q. Design of Fe_2Mo@γ-GDY triatomic catalyst for electrocatalytic urea synthesis of N_2 and CO: a theoretical study. *J. Mater. Inf.* **2025**, *5*, 11. https://dx.doi.org/10.20517/jmi.2024.49

Received: 24 Sep 2024 **First Decision:** 20 Nov 2024 **Revised:** 25 Dec 2024 **Accepted:** 30 Dec 2024 **Published:** 13 Feb 2025

Academic Editors: Fengyu Li, Yong Xu **Copy Editor:** Pei-Yun Wang **Production Editor:** Pei-Yun Wang

Abstract

While urea is widely used as a chemical raw material, its precursor ammonia (NH_3) has traditionally been synthesized under high-temperature/pressure conditions, leading to not only huge energy consumption but also serious CO_2 emission. Here, we present a groundbreaking catalyst design approach, which optimizes adsorption configurations and reaction pathways by controlling the adsorption energies of each intermediate in the reaction, thus enhancing catalytic performance. Via density functional theory (DFT) calculations, we designed a triatomic catalyst [i.e., Fe_2Mo@γ-graphdiyne (γ-GDY)] with a limiting potential of -0.22 V and a C-N coupling energy barrier of 0.34 eV. Notably, the Fe_2Mo@γ-GDY catalyst presents a high selectivity and robust antioxidation capabilities under applied potentials. Our comprehensive analysis elucidates the factors affecting the limiting potential and C-N coupling energy barrier. These insights significantly contribute to the advancement of catalyst design strategies for electrocatalytic urea synthesis, offering a more efficient and eco-friendly alternative to traditional methods.

Keywords: Electrocatalytic urea synthesis, catalyst design, transition metals, graphdiyne, density functional theory calculations

INTRODUCTION

With a notable high nitrogen content of 46%, urea [i.e., $CO(NH_2)_2$] is widely used worldwide as a nitrogen fertilizer, whose annual synthesis has exceeded 100 million tons[1]. In addition, urea has various applications, such as cosmetic formulations, synthesis of engineered wood products, and monosodium glutamate[2]. As a consequence, sustainable and efficient urea synthesis is of great importance. In the present industry, the first step of urea synthesis relies predominantly on the Haber-Bosch process for ammonia (NH_3) synthesis[3,4], which requires a high temperature (~700 K) and an elevated pressure (~100 bar). Here as well, as a second step, the energy-intensive Bosch–Meiser process that combines NH_3 with CO_2 to synthesize urea[5] necessitates elevated temperature (~423-473 K) and pressure (~150-200 bar)[6]. Annually, the entire synthesis process not only accounts for approximately 1% to 2% of total energy consumption[7], but also consumes 80% of global NH_3 synthesis[8]. Therefore, it is imperative to develop a strategy for urea synthesis with clean, environmentally friendly, energy-efficient, and resource-conserving features.

Electrocatalysis is recognized as a promising alternative[9] since it directly converts N_2 to urea under milder conditions, thereby bypassing the need for NH_3 synthesis and significantly conserving energy and resources. The electrocatalytic strategy involves the Langmuir-Hinshelwood (LH) and Eley-Rideal (ER) mechanisms [Figure 1A]. The difference between them is that N_2 and CO are co-adsorbed or not on the catalyst. Following the adsorption process, a key intermediate *NCON is formed through the C-N coupling. Then, hydrogenation of *NCON occurs gradually to form urea by the distal or the alternate mechanism. We note that the intermediate *NCON has been formed by Chen *et al.* through the LH mechanism and experimentally identified by analyzing the infrared spectrum vibration signal[10]. Over there, the energy barrier (E_b) of the C-N coupling and the maximum free energy change in the whole reaction pathway (ΔG_{max}) serve as the critical indicators for evaluating the catalyst performance. The key C-N coupling process calls for the challenging destruction of the N≡N, the transfer of CO from its adsorption site to N atoms, and the creation of a C–N bond. However, the cleavage of the N≡N is highly challenging due to its great activation energy of ~941 kJ/mol[11]. To effectively catalyze this step, the catalyst should strongly bind with N_2, aiming to fully activate the corresponding N_2. In this context, triatomic catalysts are able to act as excellent choices, where two of the constituent atoms can be designed to work in tandem to activate N_2 while the third one is optimized to weaken CO adsorption. To achieve the above goal, transition metals (TMs) can be selected due to their unfilled *d*-orbitals, which participate in a "donor-acceptor" mechanism with the adsorbate[12]. As an ideal substrate, the two-dimensional (2D) γ-graphdiyne (γ-GDY) can be used to support TMs, because it, as the most stable graphdiyne isomer[13,14], provides large pores to accommodate three TM atoms and the excellent stability and electrical conductivity[15-17].

Based on the considerations mentioned above, the selection of elements that compose TMs@γ-GDY is crucial. In conventional electrocatalyst design, researchers often use the volcano plot to select elements and design catalysts, where the adsorption energy is taken as the variant. However, this method usually considers the first and last steps of the catalytic reaction, neglecting the overall intermediate processes. With the development of electrocatalysis, we have gradually realized that the active sites in the catalytic reaction process are not fixed to one location but change during the reaction progress. Therefore, considering the intermediate steps in catalyst design is particularly important. Since intermediates in the reaction process always move towards the sites with the highest adsorption energy, we calculate the adsorption energy of the catalyst for intermediates in all the reaction steps, thereby optimizing each reaction step to promote the transfer of active sites, break the scaling relationship, and improve catalytic performance.

In this work, using density functional theory (DFT) calculations, we designed the Fe_2Mo@γ-GDY catalyst through the aforementioned design strategy. The catalyst exhibits a favorable limiting potential (U_L =

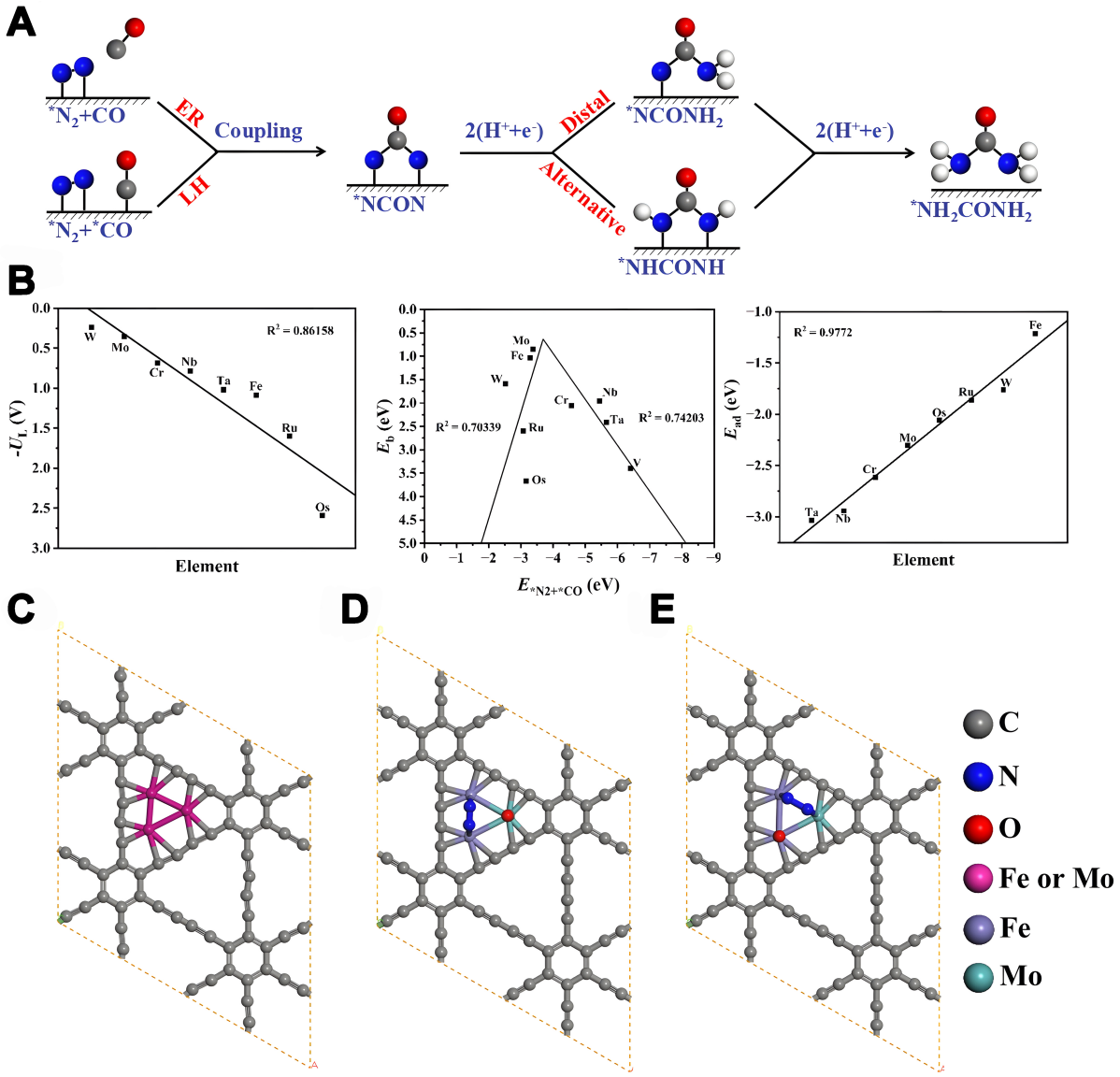

Figure 1. (A) Mechanisms of electrocatalytic synthesis of urea; (B) Curves for each element as an electrocatalyst for urea synthesis: U_L curve, $E_{ad^*N2+^*CO}$ - E_b curve for the C-N coupling process, and E_b curve for the product; (C) Doping of Fe and Mo atoms into γ-GDY; (D and E) S-type and D-type structures after doping. γ-GDY: γ-graphdiyne.

-0.22 V) and an optimized C-N coupling energy barrier (E_b = 0.34 eV). Also, a detailed discussion is carried out on how the modulation of adsorption energy affects the reduction of ΔG_{max} through the regulation of adsorption configuration and sites. Additionally, the study explores the effects of N_2 and CO adsorption on the E_b of C-N coupling. Furthermore, enhanced selectivity for hydrogen evolution reaction (HER), carbon oxygen reduction reaction (CORR), and nitrogen reduction reaction (NRR) is observed, thereby offering a strategic approach for the design of efficient catalysts in the electrocatalytic synthesis of urea.

MATERIALS AND METHODS

All spin-polarized DFT calculations were performed within the DMol^3 codes from the Materials Studio 2019 software[18]. The exchange-correlation effects were described using the Perdew-Burke-Ernzerhof (PBE) functional within the generalized gradient approximation (GGA)[19]. The Grimme method for DFT-D

correction was employed[20]. The core treatment utilized a DFT semi-core pseudopotential with a basis set of double numerical plus polarization (DNP)[21]. Convergence was accelerated by adopting smearing with a value of 0.005 Ha, while electron convergence accuracy was ensured with a real-space global orbital cutoff radius of 4.9 Å. The convergence criteria for electronic relaxation, force, and displacement were set to 10^{-5} eV, 0.002 eV/Å, and 0.005 Å, respectively. To analyze the bonding nature of the N≡N, the crystal orbital Hamilton population (COHP) analysis was performed using the Lobster software[22,23].

The substrate was modeled by a 2 × 2 monolayer of γ-GDY (18.92 × 18.92 Å^2). A vacuum of 20 Å was introduced along the *z* to avoid interactions from the periodic images in the direction normal to the substrate. Sampling of the Brillouin zone was performed using a 2 × 2 × 1 Monkhorst-Pack k-points mesh. The transition state (TS) analysis of the key intermediate (*NCON) formed by C-N coupling was implemented using the linear synchronous transit (LST)/quadratic synchronous transit (QST) method[24]. The basic parameter settings are the same as those used in other calculations, with the root mean square (RMS) convergence being set to 0.01 Ha/Å. The spin population and charge transfer were calculated using the Hirshfeld population analysis[25]. The Gibbs free energy changes for each reaction step in the electrocatalytic synthesis of urea were evaluated based on the computational hydrogen electrode (CHE) model proposed by Nørskov *et al.*[26]. Under standard reaction conditions (pH = 0, 298.15 K, and 1 atm) and at a potential of 0 V *vs.* reversible hydrogen electrode (RHE), the free energy associated with the transfer of a proton and electron pair is defined as half the value of gaseous hydrogen[27],

$$G(H^+ + e^-) = 1/2G(H_2) \tag{1}$$

The Gibbs free energy during the electrocatalytic synthesis process was calculated by

$$\Delta G = \Delta E + \Delta ZPE - T\Delta S \tag{2}$$

where ΔE represents the change of free energy obtained directly from DFT calculations, ΔZPE denotes the variation in zero-point energy, T is the Kelvin temperature (298.15 K), and ΔS indicates the change of entropy. For N_2, CO, and H_2, the *ZPE* and *S* values are obtained from the experiments[28]. The limiting potential is computed as

$$U_L = -\Delta G_{max}/e \tag{3}$$

where the variable *e* represents the number of electrons transferred during potential limiting step (PLS) and ΔG_{max} determines the PLS. The adsorption energy (E_{ad}) is calculated by

$$E_{ad} = E_{total} - E_{ads} - E^* \tag{4}$$

where E_{total} represents the total energy of the adsorption system, E_{ads} is the energy of the adsorbed species, and E^* denotes the total energy of the pristine catalyst. The mass loading of TMs atoms on the substrate of Fe_2Mo@γ-GDY is determined by

$$\eta = m_{TMs}/m_{catalyst} \times 100\% \tag{5}$$

where m_{TMs} and $m_{catalyst}$ denote the mass of Fe/Mo atoms loaded on the catalyst and the mass of the whole catalyst system, respectively. In our catalyst system, there are 72 C atoms and three TMs; therefore, m_{TMs} =

n × N_{Fe} + (3 - n) × N_{Mo}, $m_{catalyst}$ = 72 × N_C + m_{TMs}, where n represents the number of Fe atoms, and N_{Fe}, N_{Mo} and N_C are the corresponding molar mass.

RESULTS AND DISCUSSION

In the periodic table, the elements from groups V, VI, and VIII are often favored in the field of electrocatalysis due to their unique outer electron arrangements. Therefore, we select V, Cr, Fe, Nb, Mo, Ru, Ta, W, and Os as candidate elements for the catalyst design. For electrocatalytic urea synthesis, U_L, E_b, and E_{ad} of the products are critical factors. Therefore, we first calculate the U_L value for each element as a catalyst in the electrocatalytic synthesis of urea, the $E_{ad^*N2+^*CO}$ - E_b value for the C-N coupling process, and the E_{ad} value for the product [Figure 1B], and select the top three elements with the best performance. As seen in the results from Table 1, it is clear that Fe, Mo, and W present great potential. Considering that these three factors do not fully represent the entire reaction process, we also calculated the E_{ad} - ΔE curve for each reaction step in the electrocatalytic synthesis of urea using each element as a catalyst [Supplementary Figures 1-6]. Since each reaction step requires suitable ΔE and E_{ad}, we select four elements in the middle of each step's curve; the element screen is shown in Table 2. Here as well, we found that Mo, W, and Fe exhibit good performance during the reaction process. According to our design, among the three atoms, there must be both strong and weak adsorptions to allow intermediates to change configurations on the catalyst and regulate adsorption energy. In addition, considering that the melting point of W is as high as 3,400 °C, which poses an obstacle to its synthesis, we finally selected Mo and Fe for the catalyst design (here, Fe was chosen as the weak adsorption atom). We note that Fe and Mo have been widely considered as active sites to weaken the N≡N, such as the applications of $FeMo_3S_4$ and Fe/Mo-N-C in NRR[29,30]. The unoccupied *d*-orbitals of the FeMo cluster can accept lone pair electrons from N_2. Conversely, the occupied *d*-orbitals of the FeMo cluster can donate electrons to the antibonding orbitals of N_2, thereby weakening the N≡N[31]. Additionally, the synergistic interaction between Fe and Mo can significantly enhance catalytic performance. Efficient electron transfer is facilitated by the strong orbital coupling between Fe-3*d* and Mo-4*d*. This ensures not only excellent electron conduction from the catalyst to the adsorbed intermediate, but also remarkable stability of the catalyst[32]. Therefore, we select Fe and Mo loaded onto γ-GDY to form Fe_xMo_{3-x} (x = 0, 1, 2, 3) as the electrocatalyst.

Figure 1C builds a Fe_xMo_{3-x}@γ-GDY (x = 0, 1, 2, 3) model, which generates four structures: Mo_3@γ-GDY, Fe_3@γ-GDY, Fe_2Mo@γ-GDY, and $FeMo_2$@γ-GDY. Table 3 presents the calculated ΔG_{max} and E_b values for all the four cases. It is noteworthy that the electrocatalytic urea synthesis process on Fe_3@γ-GDY cannot be successfully completed. According to the findings of Zhou *et al.*[33], a lower Hirshfeld charge on N points [Supplementary Table 1] indicates weaker nucleophilicity, making N_2 less sensitive to adsorption (or alternatively, allowing H^+ to be more easily adsorbed by the underlying Fe). It is clear from Table 3 that Fe_2Mo@γ-GDY possesses excellent electrocatalytic thermodynamic and kinetic performances for urea synthesis (i.e., much lower ΔG_{max} and E_b values). Here, the excellent performance of Fe_2Mo@γ-GDY is in line with our design described in the Introduction section.

The optimal structure of Fe_2Mo@γ-GDY is shown in Figure 2A. The average bond length of the three longer edges of the C18 hexagonal hole is 6.78 Å, and the average bond length between the metal and C atoms is 2.07 Å, which is sufficient to accommodate the Fe_2Mo cluster. To assess the electronic conductivity of Fe_2Mo@γ-GDY, an essential feature for electrocatalysis, the density of states (DOS) was calculated. As shown in Figure 2B, the DOS crosses the Fermi level, which demonstrates the metallic characteristics of Fe_2Mo@γ-GDY. To explore the stability of Fe_2Mo@γ-GDY, its frequency and formation energy were evaluated. Figure 2C provides the frequency distribution for Fe_2Mo@γ-GDY, where the absence of imaginary frequencies indicates excellent stability. In addition, a negative formation energy of E_{form} =

Table 1. The screen results for three critical factors

	Candidate elements		
U_L	Cr	Mo	W
$E_{ad*N2+*CO} - E_b$	Fe	Mo	W
E_{ad}	Fe	Ru	W

Table 2. The screen results for each reaction step

Step	Candidate elements			
$^*N_2 - {}^*N_2 + {}^*CO$	Cr	Nb	Mo	Ta
$^*N_2 + {}^*CO - {}^*NCON$	Cr	Nb	Mo	W
$^*NCON - {}^*NCONH$	Cr	Fe	Mo	W
$^*NCONH - {}^*NCONH_2$	Fe	Mo	W	Os
$^*NCONH_2 - {}^*HNCONH_2$	Cr	Nb	Mo	Os
$^*HNCONH_2 - {}^*H_2NCONH_2$	Cr	Nb	Mo	Ta

Table 3. ΔG_{max} and E_b of the structures

Structure	Rate determining step	ΔG_{max} (eV)	E_b (eV)
Fe_3@γ-GDY	-	-	2.66
Fe_2Mo@γ-GDY	$^*HNCONH_2 \rightarrow {}^*H_2NCONH_2$	0.22	0.34
$FeMo_2$@γ-GDY	$^*HNCONH_2 \rightarrow {}^*H_2NCONH_2$	0.62	0.70
Mo_3@γ-GDY	$^*HNCONH_2 \rightarrow {}^*H_2NCONH_2$	0.91	1.44

γ-GDY: γ-graphdiyne.

-0.49 eV again demonstrates the stability of Fe_2Mo@γ-GDY. Furthermore, the ab initio molecular dynamics (AIMD) simulations within the canonical ensemble (NVT) at a temperature of 300 K were performed to further evaluate the dynamic stability under aqueous conditions. The time step was set to 1.0 fs and the total simulation time was set to 10.0 ps. The thermostat was set to Massive GGM, with a chain length of 2, a relaxation time of 10.0, and a Yoshida parameter of 3. It is clear from the snapshots of Fe_2Mo@γ-GDY at 0, 2, 4, 6, 8 and 10 ps [Figure 2D] that the structural deformation is insignificant.

The theoretical feasibility of triatomic doping in graphene has been proposed[34]. The distinctive *sp*-hybridized triple bond structure of γ-GDY suggests significant advantages in anchoring surface metal atoms[35]. Moreover, triatomic doping in similar 2D materials has been realized. For instance, Wang *et al.* successfully synthesized the CNT@C_3N_4-Fe_2Cu catalyst, where Fe and Cu were predominantly loaded as triatomic clusters[36]. In particular, CNT@C_3N_4-Fe_2Cu exhibits an 18.3% mass loading rate of metal atoms, while the Fe_2Mo@γ-GDY model presents 19.4%, which denotes a reasonable design of metal atom loading in our study. Based on the experimental results of CNT@C_3N_4-Fe_2Cu, we design a feasible experimental method for the fabrication of Fe_2Mo@γ-GDY: forming intermediate products between γ-GDY and precursor containing Mo and Fe by hydrothermal method and annealing them to produce Fe_2Mo@γ-GDY in the atmosphere of H_2 and Ar.

The adsorption of N_2 on Fe_2Mo@γ-GDY has two possible configurations: the S-type (Fe_2Mo-S@γ-GDY, Figure 1D) with N_2 on two identical atoms and the D-type with N_2 on two distinct atoms (Fe_2Mo-D@γ-GDY, Figure 1E). In order to reveal optimal adsorption configuration, the E_{coad} values of Fe_2Mo-S@γ-GDY (-0.35 eV) and Fe_2Mo-D@γ-GDY (-2.21 eV) were calculated. Obviously, N_2 always

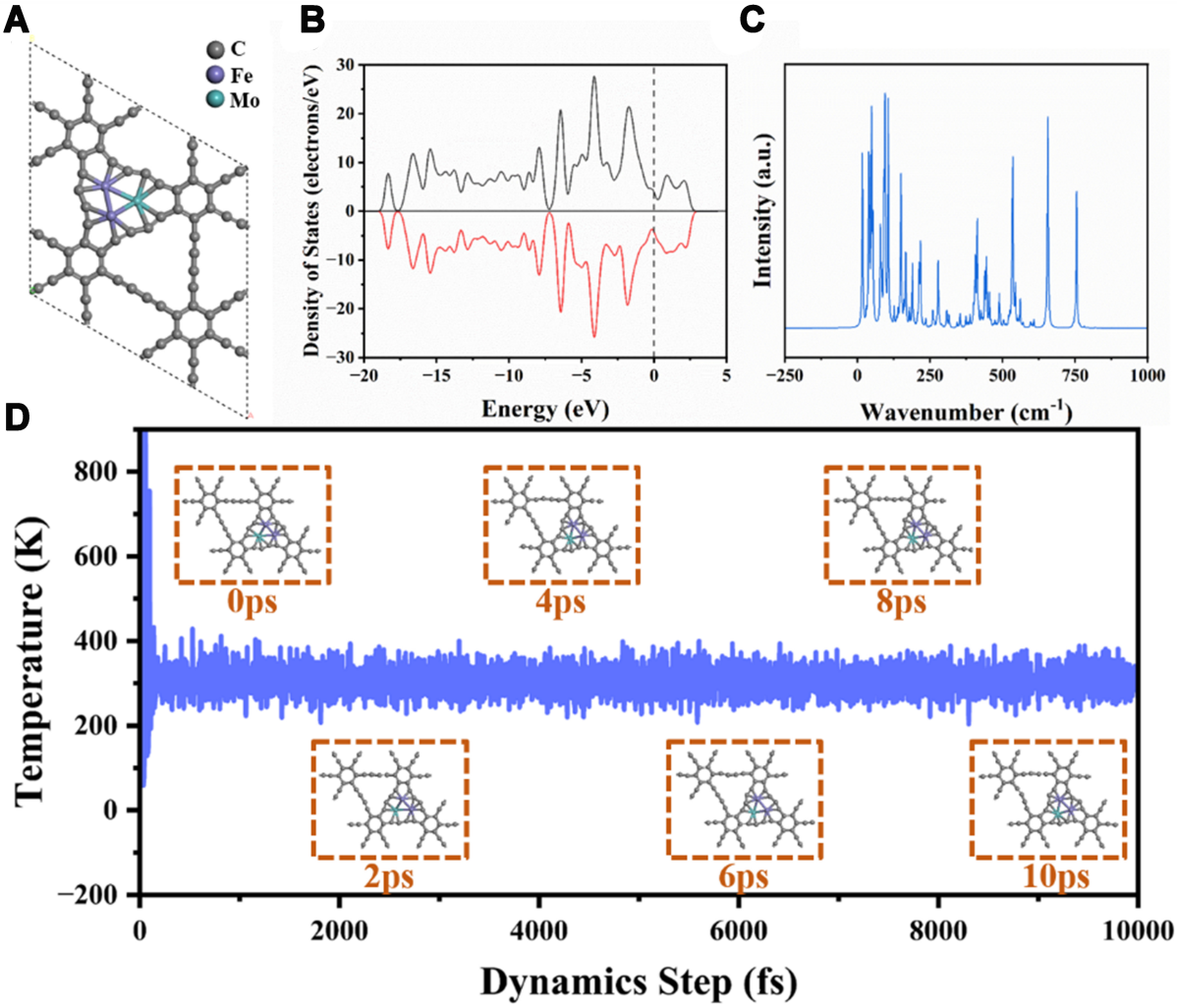

Figure 2. (A) Optimized structures of Fe_2Mo@γ-GDY; (B) DOS of Fe_2Mo@γ-GDY with the Fermi level set at 0 eV, where the black and red lines represent spin up and spin down, respectively; (C) Frequency of Fe_2Mo@γ-GDY; (D) AIMD simulation of Fe_2Mo-D@γ-GDY at the temperature of 300 K under aqueous conditions. γ-GDY: γ-graphdiyne; DOS: density of states.

preferentially adsorbs on Fe_2Mo-D@γ-GDY (hereafter, Fe_2Mo@γ-GDY will refer to Fe_2Mo-D@γ-GDY). The mechanism of electrocatalytic urea synthesis on Fe_2Mo@γ-GDY involves four reaction pathways: LH and ER mechanisms during the C-N coupling and distal and alternative mechanisms during the proton-coupled electron transfer (PCET) steps. Given that the reaction pathways initially involve LH and ER mechanisms, the corresponding E_b values calculated are 0.34 and 0.64 eV, respectively, indicating the more favorable LH mechanism for the C-N coupling. Namely, N_2 and CO are firstly co-adsorbed on the Fe_2Mo@γ-GDY catalyst, followed by the formation of *NCON via the C-N coupling. Then, the *NCON transforms gradually to urea through the PCET steps via either the distal or the alternating mechanism. The ΔG_{max} value for the alternative mechanism is 0.22 eV, lower than 0.30 eV for the distal mechanism. Overall, the electrocatalytic urea synthesis process on Fe_2Mo@γ-GDY will proceed with the LH and alternative mechanisms.

To investigate the activation of N_2, we conducted a comprehensive analysis by calculating the partial DOS (PDOS) before and after N_2 adsorption [Figure 3A]. The findings reveal a remarkable alignment between the 2*s* and 2*p* orbitals of N_2 and the *d*-orbitals of Fe_2Mo, indicating a pronounced hybridization between N_2

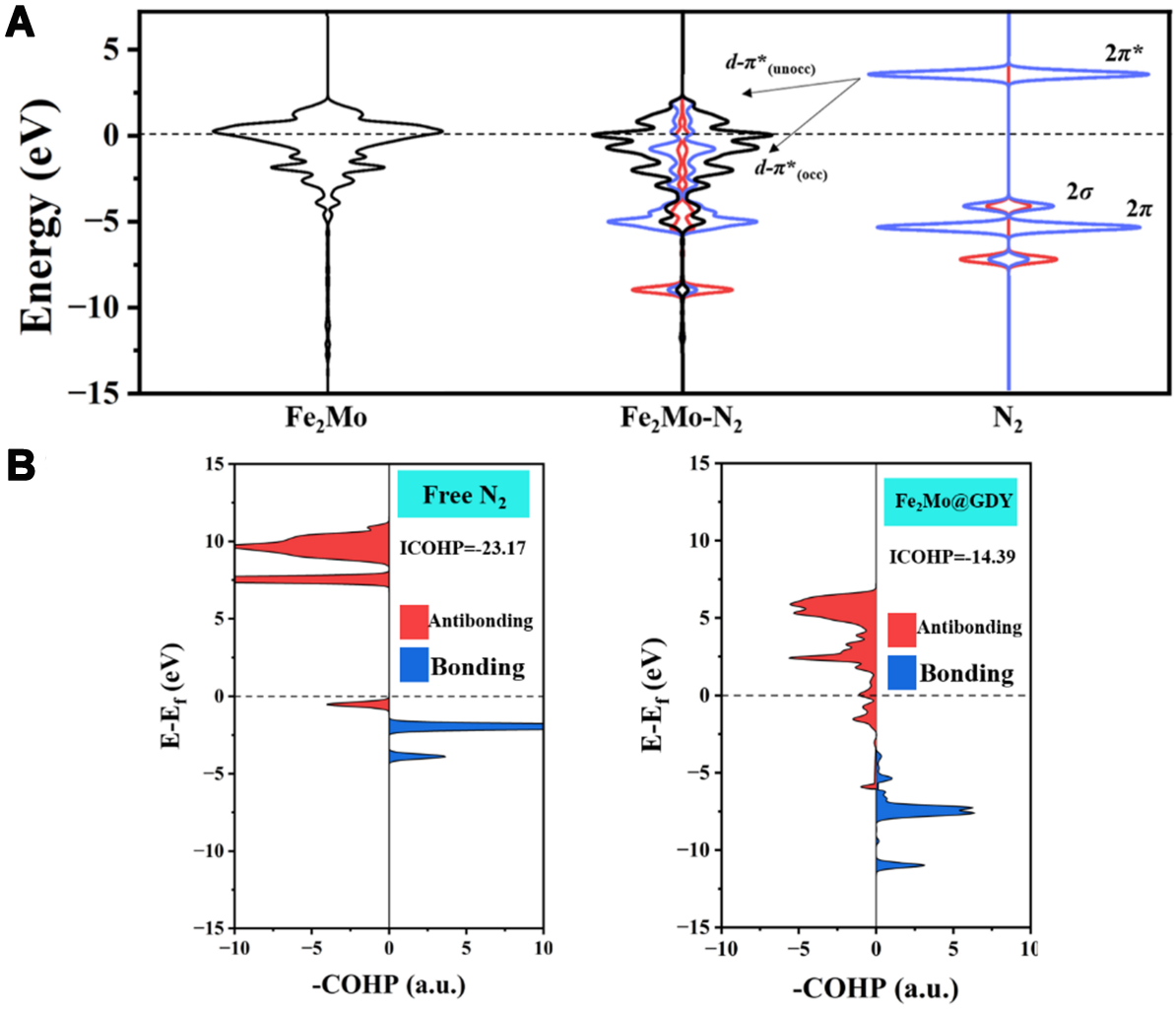

Figure 3. (A) PDOS of Fe_2Mo, N_2 adsorbed at hollow site on Fe_2Mo@γ-GDY, and free N_2 molecule, surface. The black, blue, and red lines represent the outermost *d* orbitals, *p* orbitals, and *s* orbitals of the corresponding structures, respectively; (B) COHP for N≡N bond of free N_2 molecule, adsorbed N_2 on Fe_2Mo@γ-GDY. PDOS: Partial density of states; γ-GDY: γ-graphdiyne; COHP: crystal orbital Hamilton population.

and Fe_2Mo. Subsequent to this hybridization, a portion of the unoccupied $2\pi^*$ orbitals of N_2 falls below the Fermi level, signifying their partial occupation by the *d*-orbitals of Fe_2Mo. This observation supports the notion of a substantial electron transfer between Fe_2Mo and N_2, ultimately leading to the activation of the N≡N. The activated N≡N species demonstrate enhanced propensity to form a $2N^*$ adsorption state on the catalyst surface, thereby facilitating the C-N coupling process and reducing the E_b. Furthermore, the COHP for $^*N_2$ on Fe_2Mo@γ-GDY and pure N_2 molecule are analyzed [Figure 3B], where red and blue areas represent the antibonding and bonding contributions, respectively. Here, the integrated COHP (ICOHP) can quantitatively describe the strength of N≡N, in which a less negative ICOHP value corresponds to a weaker N≡N[37]. It is obvious that Fe_2Mo@γ-GDY weakens the N≡N.

During the protonation process, *NCON and *NCONH are adsorbed by Fe_2Mo@γ-GDY at the hollow site. Then, *HNCONH and $^*H_2$NCONH are located by Fe_2Mo@γ-GDY at the bridge site. Finally, the adsorbed intermediate ($^*H_2NCONH_2$) undergoes a transition from the bridge site to the top site. Analysis of intermediate adsorption energies reveals a dynamic shift during the reaction process, facilitating a transition

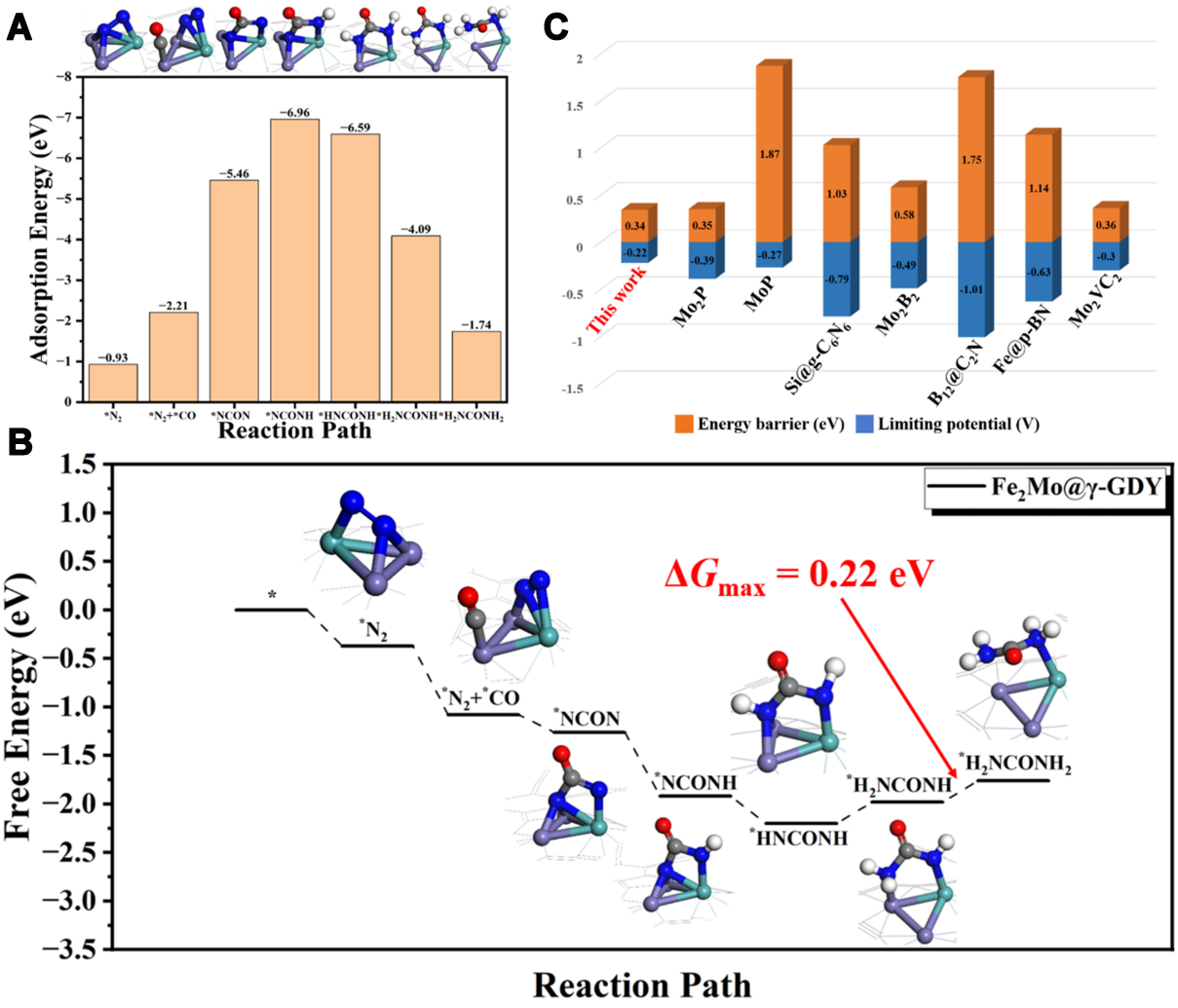

Figure 4. (A) Evolution of adsorption energy; (B) Free energy step on Fe_2Mo@γ-GDY; (C) Performance comparison. γ-GDY: γ-graphdiyne.

from a weaker to a stronger adsorption site. During the reaction, active sites relocate throughout the process, disrupting the scaling relationship[38] and leading to a reduction in reaction-free energy[39]. From the evolution of adsorption energy for the entire process [Figure 4A], it can be seen that the initial adsorption energy of the protonation step is the strongest. This robust initial adsorption favors H^+ binding, promoting the reaction and enhancing adsorption capacity for later H^+ binding events. Subsequently, the adsorption energy gradually diminishes, culminating in adsorption at top site. This shift is conducive to reaction termination, facilitating the easy desorption of formed urea molecules from the reaction site. This enables the catalyst to progress seamlessly to the subsequent synthesis steps. The ΔG value at each step is shown in Figure 4B. It is worth stressing that the electrocatalytic performance of Fe_2Mo@γ-GDY is superior to other catalysts reported in the DFT-based studies on urea synthesis, as compared in Figure 4C[40-46].

At this stage, the selectivity of Fe_2Mo@γ-GDY is considered. The competitive reactions of the electrocatalytic synthesis of urea mainly include the HER, CORR, and NRR; their structural diagrams are shown in Supplementary Figures 7-9. For HER, we analyzed the H^+ competition in each reaction step prior to the protonation step. For the first and second steps, which relate to adsorption processes, the adsorption

energies were used for comparison. For the C-N coupling process, the changes in free energy were used for comparison. For * - $^*N_2$, the E_{ad} of the catalyst for N_2 is -0.93 eV, while for H^+, it is only -0.23 eV; for $^*N_2$ - $^*N_2$ + $^*CO$, the E_{ad} for CO is -1.28 eV, while for H^+, it is a positive value of 0.06 eV; for $^*N_2$ + $^*CO$ - $^*NCON$, ΔG for the C-N coupling is -0.18 eV. The formation of $^*N_2H$ + $^*CO$ has a ΔG value of 0.17 eV, and the formation of $^*N_2$ + $^*COH$ has a ΔG value of -0.06 eV. Therefore, HER is difficult to occur. There are two paths for the first hydrogenation of CORR[47]. One is the COH formation by hydrogenation on O, and the other is the CHO formation by hydrogenation on C. The free energy values of the two pathways from $^*N_2$ + $^*CO$ are -0.06 and 1.17 eV, respectively. Both are higher than the C-N coupling process (-0.18 eV). As to NRR, the free energy for forming $^*NNH$ + $^*CO$ is 0.00 eV, which is higher than the free energy of C-N coupling (-0.18 eV), indicating that retrograde C-N coupling is more preferred. The reaction free energy profile for NRR is depicted in Supplementary Figure 9, where ΔG_{max} equals 0.63 eV, significantly higher than that of urea synthesis (0.22 eV). Thus, Fe_2Mo@γ-GDY has a good selectivity for electrocatalytic urea synthesis.

CONCLUSIONS

We have designed a triatomic Fe_2Mo@γ-GDY catalyst for the electrochemical synthesis of urea by regulating the adsorption energy and adsorption configuration for each step of the reaction process. Through DFT calculations, we have demonstrated that this catalyst possesses good stability and electronic conductivity. The catalyst not only gives an excellent catalytic performance in theoretical calculations (U_L = -0.22 V, E_b = 0.34 eV), but also shows a good selectivity through various evaluation metrics. Additionally, the catalyst exhibits strong antioxidative performance under operational potentials. Compared to the current methods of urea synthesis under high-temperature and high-pressure conditions, the Fe_2Mo@γ-GDY catalyst offers a viable route for synthesizing urea under ambient conditions. Overall, the Fe_2Mo@γ-GDY catalyst provides a new and more sustainable method for the electrocatalytic synthesis of urea, and it is expected to replace traditional energy-intensive synthesis methods in future industrial applications.

DECLARATIONS

Acknowledgments

We acknowledge the financial support from the National Natural Science Foundation of China (No. 52130101), the "World-class Universities and World-class Disciplines" fund, China, the National Key R&D Program of China (No. 2023YFB3003001), and the "Xiaomi Young Scholar" Project.

Authors' contributions

Conceived and designed the DFT calculations: Wang, T.; Jiang, Q.
Performed DFT calculations and the related analysis: Chi, L.; Wang, T.
Wrote the paper, discussed the results, and commented on the manuscript: Chi, L.; Wang, T.; Jiang, Q.

Availability of data and materials

The data supporting our findings can be found in the Supplementary Materials.

Financial support and sponsorship

This work was financially supported by the National Natural Science Foundation of China (No. 52130101), the "World-class Universities and World-class Disciplines" fund, China, the National Key R&D Program of China (No. 2023YFB3003001), and the "Xiaomi Young Scholar" Project.

Conflicts of interest

Jiang, Q. serves as an Associate Editor for *Journal of Materials Informatics*. However, Jiang, Q. was not involved in any aspect of the editorial process for this manuscript, including reviewer selection, manuscript handling, or decision-making. The remaining authors declare no conflicts of interest.

Ethical approval and consent to participate

Not applicable.

Consent for publication

Not applicable.

REFERENCES

1. Geng, J.; Ji, S.; Jin, M.; et al. Ambient electrosynthesis of urea with nitrate and carbon dioxide over iron-based dual-sites. *Angew. Chem. Int. Ed. Engl.* **2023**, *62*, e202210958. DOI PubMed PMC
2. Celleno, L. Topical urea in skincare: a review. *Dermatol. Ther.* **2018**, *31*, e12690. DOI PubMed
3. Sun, C. N.; Wang, Z. L.; Lang, X. Y.; Wen, Z.; Jiang, Q. Synergistic effect of active sites of double-atom catalysts for nitrogen reduction reaction. *ChemSusChem* **2021**, *14*, 4593-600. DOI
4. Dai, T.; Lang, X.; Wang, Z.; Wen, Z.; Jiang, Q. Rational design of an Fe cluster catalyst for robust nitrogen activation. *J. Mater. Chem. A.* **2021**, *9*, 21219-27. DOI
5. Wei, X.; Liu, Y.; Zhu, X.; et al. Dynamic reconstitution between copper single atoms and clusters for electrocatalytic urea synthesis. *Adv. Mater.* **2023**, *35*, e2300020. DOI
6. Lv, C.; Lee, C.; Zhong, L.; et al. A defect engineered electrocatalyst that promotes high-efficiency urea synthesis under ambient conditions. *ACS. Nano.* **2022**, *16*, 8213-22. DOI
7. Jiang, M.; Zhu, M.; Wang, M.; et al. Review on electrocatalytic coreduction of carbon dioxide and nitrogenous species for urea synthesis. *ACS. Nano.* **2023**, *17*, 3209-24. DOI
8. Erisman, J. W.; Sutton, M. A.; Galloway, J.; Klimont, Z.; Winiwarter, W. How a century of ammonia synthesis changed the world. *Nature. Geosci.* **2008**, *1*, 636-9. DOI
9. Huang, Y.; Wang, Y.; Liu, Y.; et al. Unveiling the quantification minefield in electrocatalytic urea synthesis. *Chem. Eng. J.* **2023**, *453*, 139836. DOI
10. Chen, C.; Zhu, X.; Wen, X.; et al. Coupling N_2 and CO_2 in H_2O to synthesize urea under ambient conditions. *Nat. Chem.* **2020**, *12*, 717-24. DOI
11. Sun, C. N.; Qu, Y. B.; Wang, Z. L.; Jiang, Q. Hydrogen spillover in alkaline solutions for effective nitrogen fixation. *Chem. Eng. J.* **2023**, *471*, 144589. DOI
12. Yang, L.; Feng, S.; Zhu, W. Novel honeycomb-like metal organic frameworks as multifunction electrodes for nitrate degradation: A computational study. *J. Hazard. Mater.* **2023**, *445*, 130534. DOI
13. Lu, Z.; Li, S.; Lv, P.; He, C.; Ma, D.; Yang, Z. First principles study on the interfacial properties of NM/graphdiyne (NM = Pd, Pt, Rh and Ir): the implications for NM growing. *Appl. Surf. Sci.* **2016**, *360*, 1-7. DOI
14. Song, B.; Chen, M.; Zeng, G.; et al. Using graphdiyne (GDY) as a catalyst support for enhanced performance in organic pollutant degradation and hydrogen production: a review. *J. Hazard. Mater.* **2020**, *398*, 122957. DOI
15. Fang, Y.; Liu, Y.; Qi, L.; Xue, Y.; Li, Y. 2D graphdiyne: an emerging carbon material. *Chem. Soc. Rev.* **2022**, *51*, 2681-709. DOI
16. Li, L.; Qiao, W.; Bai, H.; Huang, Y. Structural and electronic properties of α-, β-, γ-, and 6,6,18-graphdiyne sheets and nanotubes. *RSC. Adv.* **2020**, *10*, 16709-17. DOI PubMed PMC
17. Li, Y.; Xu, L.; Liu, H.; Li, Y. Graphdiyne and graphyne: from theoretical predictions to practical construction. *Chem. Soc. Rev.* **2014**, *43*, 2572-86. DOI
18. Delley, B. From molecules to solids with the DMol3 approach. *J. Chem. Phys.* **2000**, *113*, 7756-64. DOI
19. Perdew, J. P.; Burke, K.; Ernzerhof, M. Generalized gradient approximation made simple. *Phys. Rev. Lett.* **1996**, *77*, 3865-8. DOI PubMed
20. Grimme, S. Semiempirical GGA-type density functional constructed with a long-range dispersion correction. *J. Comput. Chem.* **2006**, *27*, 1787-99. DOI PubMed
21. Delley, B. Hardness conserving semilocal pseudopotentials. *Phys. Rev. B.* **2002**, *66*, 155125. DOI
22. Dronskowski, R.; Bloechl, P. E. Crystal orbital Hamilton populations (COHP): energy-resolved visualization of chemical bonding in solids based on density-functional calculations. *J. Phys. Chem.* **1993**, *97*, 8617-24. DOI
23. Deringer, V. L.; Tchougréeff, A. L.; Dronskowski, R. Crystal orbital Hamilton population (COHP) analysis as projected from plane-wave basis sets. *J. Phys. Chem. A.* **2011**, *115*, 5461-6. DOI PubMed
24. Halgren, T. A.; Lipscomb, W. N. The synchronous-transit method for determining reaction pathways and locating molecular transition states. *Chem. Phys. Lett.* **1977**, *49*, 225-32. DOI
25. Hirshfeld, F. L. Bonded-atom fragments for describing molecular charge densities. *Theoret. Chim. Acta.* **1977**, *44*, 129-38. DOI
26. Nørskov, J. K.; Rossmeisl, J.; Logadottir, A.; et al. Origin of the overpotential for oxygen reduction at a fuel-cell cathode. *J. Phys. Chem. B.* **2004**, *108*, 17886-92. DOI

27. Skúlason, E.; Bligaard, T.; Gudmundsdóttir, S.; et al. A theoretical evaluation of possible transition metal electro-catalysts for N_2 reduction. *Phys. Chem. Chem. Phys.* **2012**, *14*, 1235-45. DOI
28. Haynes, W. M. CRC handbook of chemistry and physics. 97th edition. CRC Press, 2016. DOI
29. Zhu, P.; Xiong, X.; Wang, X.; et al. Regulating the FeN_4 moiety by constructing Fe-Mo dual-metal atom sites for efficient electrochemical oxygen reduction. *Nano. Lett.* **2022**, *22*, 9507-15. DOI
30. Gao, S.; Liu, X.; Wang, Z.; et al. Spin regulation for efficient electrocatalytic N_2 reduction over diatomic Fe-Mo catalyst. *J. Colloid. Interface. Sci.* **2023**, *630*, 215-23. DOI
31. Zhang, Y.; Ma, N.; Wang, Y.; Liang, B.; Fan, J. Theoretical design toward highly efficient single-atom catalysts for nitrogen reduction by regulating the "acceptance-donation" mechanism. *Appl. Surf. Sci.* **2023**, *623*, 156827. DOI
32. Hu, J.; Zhang, C.; Sun, M.; et al. Ultrastable bimetallic Fe_2Mo for efficient oxygen reduction reaction in pH-universal applications. *Nano. Res.* **2022**, *15*, 4950-7. DOI
33. Zhou, X. Y.; Rong, C. Y.; Lu, T.; Liu, S. B. Hirshfeld charge as a quantitative measure of electrophilicity and nucleophilicity: nitrogen-containing systems. *Acta. Phys. Chim. Sin.* **2014**, *30*, 2055-62. DOI
34. Chen, Z. W.; Chen, L. X.; Jiang, M.; et al. A triple atom catalyst with ultrahigh loading potential for nitrogen electrochemical reduction. *J. Mater. Chem. A.* **2020**, *8*, 15086-93. DOI
35. Liang, S.; Deng, H.; Zhou, Z.; Wong, W. Fabrication of graphdiyne and its analogues for photocatalytic application. *EcoMat* **2023**, *5*, e12297. DOI
36. Wang, X.; Qiu, S.; Feng, J.; et al. Confined Fe-Cu clusters as sub-nanometer reactors for efficiently regulating the electrochemical nitrogen reduction reaction. *Adv. Mater.* **2020**, *32*, e2004382. DOI
37. Zhou, H. Y.; Qu, Y. B.; Li, J. C.; Wang, Z. L.; Yang, C. C.; Jiang, Q. Effectively boosting selective ammonia synthesis on electron-deficient surface of MoB_2. *Appl. Catal. B. Environ.* **2022**, *305*, 121023. DOI
38. Zhang, J.; Yang, H. B.; Zhou, D.; Liu, B. Adsorption energy in oxygen electrocatalysis. *Chem. Rev.* **2022**, *122*, 17028-72. DOI
39. Govindarajan, N.; García-Lastra, J. M.; Meijer, E. J.; Calle-Vallejo, F. Does the breaking of adsorption-energy scaling relations guarantee enhanced electrocatalysis? *Curr. Opin. Electrochem.* **2018**, *8*, 110-7. DOI
40. Jiao, D.; Wang, Z.; Liu, Y.; et al. Mo_2P Monolayer as a superior electrocatalyst for urea synthesis from nitrogen and carbon dioxide fixation: a computational study. *Energy. Environ. Mater.* **2024**, *7*, e12496. DOI
41. Jiao, D.; Dong, Y.; Cui, X.; et al. Boosting the efficiency of urea synthesis *via* cooperative electroreduction of N_2 and CO_2 on MoP. *J. Mater. Chem. A.* **2022**, *11*, 232-40. DOI
42. Roy, P.; Pramanik, A.; Sarkar, P. Dual-silicon-doped graphitic carbon nitride sheet: an efficient metal-free electrocatalyst for urea synthesis. *J. Phys. Chem. Lett.* **2021**, *12*, 10837-44. DOI PubMed
43. Zhu, X.; Zhou, X.; Jing, Y.; Li, Y. Electrochemical synthesis of urea on MBenes. *Nat. Commun.* **2021**, *12*, 4080. DOI PubMed PMC
44. Cao, Y.; Meng, Y.; An, R.; et al. Revealing electrocatalytic C-N coupling for urea synthesis with metal-free electrocatalyst. *J. Colloid. Interface. Sci.* **2023**, *641*, 990-9. DOI
45. Kong, L.; Jiao, D.; Wang, Z.; et al. Single metal atom anchored on porous boron nitride nanosheet for efficient collaborative urea electrosynthesis: a computational study. *Chem. Eng. J.* **2023**, *451*, 138885. DOI
46. Yang, Y.; Peng, J.; Shi, Z.; Zhang, P.; Arramel, A.; Li, N. Unveiling the key intermediates in electrocatalytic synthesis of urea with CO_2 and N_2 coupling reactions on double transition-metal MXenes. *J. Mater. Chem. A.* **2023**, *11*, 6428-39. DOI
47. Liang, F.; Zhang, K.; Zhang, L.; Zhang, Y.; Lei, Y.; Sun, X. Recent development of electrocatalytic CO_2 reduction application to energy conversion. *Small* **2021**, *17*, e2100323. DOI